Physics of Plasmas

On the rate of energy deposition by an ion ring velocity beam

Cite as: Phys. Plasmas **28**, 052102 (2021); https://doi.org/10.1063/5.0046309
Submitted: 02 February 2021 . Accepted: 03 April 2021 . Published Online: 03 May 2021

Yuri A. Omelchenko, Leonid Rudakov, Jonathan Ng, Chris Crabtree, and Gurudas Ganguli

Physics of Plasmas ARTICLE scitation.org/journal/php

On the rate of energy deposition by an ion ring velocity beam

Cite as: Phys. Plasmas **28**, 052102 (2021); doi: 10.1063/5.0046309
Submitted: 2 February 2021 · Accepted: 3 April 2021 ·
Published Online: 3 May 2021

Yuri A. Omelchenko,[1,a)] Leonid Rudakov,[1] Jonathan Ng,[2,3] Chris Crabtree,[4] and Gurudas Ganguli[4]

AFFILIATIONS

[1]Trinum Research, Inc., San Diego, California 92126, USA
[2]University of Maryland, College Park, Maryland 20742, USA
[3]NASA Goddard Space Flight Center, Greenbelt, Maryland 20771, USA
[4]Plasma Physics Division, Naval Research Laboratory, Washington, DC 20375, USA

[a)]Author to whom correspondence should be addressed: omelche@gmail.com

ABSTRACT

Using a novel three-dimensional electromagnetic hybrid code, XHYPERS, we simulate the generation of lower hybrid oscillations in a magnetized plasma by a heavy ion beam with a ring-shaped velocity distribution over much longer periods of time compared to previous simulations. We introduce a phenomenological (effective) electron damping to represent the induced scattering of lower-hybrid waves to whistlers and the loss of energy through whistler propagation out of the turbulent region. We demonstrate the effective electron damping to be a crucial factor in increasing the efficiency of energy deposition by an ion ring velocity beam into plasma turbulence and investigate the efficiency of beam energy extraction as a function of the electron damping rate and beam to plasma ion mass ratio.

I. INTRODUCTION

The ability of an ion beam with a ring velocity distribution to generate lower hybrid plasma turbulence in a magnetized plasma has significant implications for space and laboratory plasma applications.[1–4] In particular, the upcoming Space Measurement of A Rocket-Released Turbulence (SMART) mission is designed to understand the evolution of ion beam generated plasma turbulence and its nonlocal electrostatic/electromagnetic nature.[5,6]

The initial source of energy in the beam-plasma system in the SMART experiment is the kinetic energy of photo-ionized barium (Ba) neutrals, transversely injected into the ambient magnetic field and eventually forming a ring-shaped drifting Maxwellian distribution in velocity space. To anticipate the outcome of space experiments, it is important to be able to estimate the amount of energy deposited by an ion ring velocity beam into the generation of electrostatic lower hybrid waves. These waves, driven by a Ba cloud to be released from a satellite in the upper ionosphere, are predicted to evolve nonlinearly into electromagnetic whistler waves, which then may propagate into the magnetosphere similarly to whistler waves commonly generated by lightnings.[2,5]

A detailed theoretical analysis of the linear[7] and nonlinear[3] ion beam evolution as well as the three-dimensional (3D) properties of the beam generated turbulence[8] suggests that nonlinear processes, such as the induced scattering of electrostatic lower hybrid waves by thermal electrons and the subsequent conversion of electrostatic wave turbulence to electromagnetic whistler waves, play a crucial role as the dominant wave saturation mechanisms at later stages of the quasilinear beam evolution.[9] The SMART experiment represents an excellent venue for verifying these theoretical conclusions obtained in the framework of weak turbulence theory.[5]

In anticipation of the detailed results from the upcoming space experiments, a number of laboratory and computational studies have been performed to advance the knowledge of nonlinear beam interactions with the ambient plasma. The experiment conducted in the Space Physics Simulation Chamber at the Naval Research Laboratory[4,10] demonstrated the conversion of electrostatic lower hybrid (pump) waves to electromagnetic waves through induced scattering by thermal electrons. Two-dimensional (2D) hybrid simulations[11] investigated the ion ring beam interaction with a magnetoplasma in the electrostatic limit. Importantly, the 2D electrostatic hybrid model included effective collisions to phenomenologically account for the conversion of electrostatic oscillations to electromagnetic waves and their subsequent convection out of the localized beam region. These simulations demonstrated a significant increase in the efficiency of extraction of energy from the ion beam over that predicted in the absence of effective electron motion damping.[11]

Recently, 2D electrostatic particle-in-cell (PIC) simulations were carried out to study the early time behavior of the SMART experiment.[6] These simulations were limited to understanding the neutral barium injection, photoionization of the neutrals to form the ring distribution, and the consequent generation of the electrostatic lower hybrid waves. For these early time dynamics, a 2D electrostatic simulation model is sufficient. Accordingly, the duration of validity of these simulations to the realistic SMART experiment is until the time when the wave energy density becomes sufficiently large so that the nonlinear (induced scattering) damping rate and the beam instability growth rate become of the same order. Beyond this time, a 3D electromagnetic PIC model with radiative boundary conditions or a hybrid model with a parameterized representation of nonlinear scattering is necessary. In this paper, for computational efficiency (as explained below) we adopt the latter approach and focus on the late time dynamics of the ring instability.

The most comprehensive numerical studies of the generation of plasma turbulence by an ion ring velocity beam to date were performed using full particle-in-cell (PIC) simulations in two and three dimensions.[12,13] In particular, the 2D full PIC simulations, ignoring the third spatial dimension perpendicular to the ambient magnetic field, revealed that the ion beam distribution relaxes in velocity space asymmetrically. This simulation artifact was shown to lead to (i) a multi-peak excitation of lower hybrid waves; (ii) an increased (by an order of magnitude) level of turbulence energy compared to the 3D simulations; and (iii) a stepwise rate of energy extraction vs a gradually falling function observed in 3D. These 2D geometry-induced artifacts make it difficult to correctly estimate energy losses by an ion ring velocity beam over longer periods of time.

Further, the 3D full PIC simulations[12,13] have demonstrated a loss of beam energy of order $\sim$5% by the end of simulation time, $\omega_{pi}t \simeq 800$, where ω_{pi} is the background (bulk) ion plasma frequency. The lower hybrid waves saturated in the 3D simulations at a significantly lower level compared to the 2D simulations, which was manifested in much less developed density striations in the 3D case. In contrast to the 2D electrostatic simulations,[11] these full PIC simulations did not account for wave convection out of the beam-plasma system.

It was also noted by Winske and Daughton[12] that because of the inherent noise generated by the finite-size particles, the full PIC simulations in question may not be capable of fully resolving induced electron scattering effects fundamental to the nonlinear theory of ion beam evolution.[3,8] However, subsequent detailed analysis of the presented simulation results supported the general picture that the instability was saturated at a lower level by nonlinear induced scattering with wave-vectors of electromagnetic fluctuations consistent with the expected scattered waves.[14]

The geometry-dependent relaxation of the ion beam in the 2D electrostatic simulations and the computational limitations of the full PIC model have motivated us to conduct new, much longer 3D simulations of the beam-plasma system. This is accomplished with a novel, electromagnetic hybrid approach where the plasma electrons are represented as a cold fluid with phenomenological damping, and the ion components (here the beam and background plasma ions) are modeled as macro-particles.

In Sec. II, we describe our electromagnetic hybrid model. In Sec. III, we discuss the results from 3D hybrid simulations of the ion beam-system. Finally, our conclusions are summarized in Sec. IV.

II. COMPUTATIONAL MODEL

In this work, we employ an extended 3D version of the HYPERS code,[15] XHYPERS. The standard hybrid (HYPERS) model neglects the displacement current in Maxwell's equations, assumes the quasi-neutral fluid approximation for the inertialess plasma electrons and treats the ion species as the kinetic macro-particles. While this model is sufficient for many space[15] and laboratory[16] plasma applications, it needs to be further extended to include lower-hybrid oscillations in ion ring instability studies.

A. Extended hybrid model: Equations

Finite electron mass (m_e) effects can be introduced into the standard hybrid model in a variety of ways. For instance, for magnetic reconnection studies these effects were accounted for by retaining the advection term in the electron equation of motion and using the modified Faraday law.[17] More recently, a modified version of this approach was used to enable robust hybrid calculations in vacuum at the expense of solving an elliptic equation for electric field.[18] A finite-mass fluid description for the cold electron component was also used to simulate whistlers in the Darwin limit.[19]

Here, we employ a non-Darwin approximation, similar in spirit to one previously used to derive an extended magnetohydrodynamics (XMHD) model for simulating plasma jets and shocks in laboratory experiments.[20] This approach takes into account radiation effects that are essential for describing the dispersion of oblique whistlers. Currently, we also assume charge quasineutrality, which has a large domain of applicability, including the lower-hybrid instability.

The full set of equations solved by the XHYPERS model is as follows:

$$m_e\left[\frac{\partial \mathbf{V}_e}{\partial t} + (\mathbf{V}_e \cdot \nabla)\mathbf{V}_e\right] = -e\left[\mathbf{E} + \frac{\mathbf{V}_e \times \mathbf{B}}{c}\right] - \nu_e m_e \mathbf{V}_e, \quad (1)$$

$$\frac{1}{c}\frac{\partial \mathbf{E}}{\partial t} = \frac{4\pi}{c}(en_e\mathbf{V}_e - \mathbf{J}_i) + \nabla \times \mathbf{B}, \quad (2)$$

$$\frac{\partial \mathbf{B}}{\partial t} = -c\nabla \times \mathbf{E}, \quad (3)$$

$$en_e = \rho_i. \quad (4)$$

In Eqs. (1)–(4), ρ_i and $\mathbf{J}_i$ are the net ion charge and current densities calculated from ion macro-particle distributions; e and c are the absolute value of electron charge and speed of light; $n_e, \mathbf{V}_e, \nu_e$ are the fluid electron number density, velocity, and effective collision frequency, respectively; and $\mathbf{E}$, $\mathbf{B}$ are the electric and magnetic fields.

The multiple ion components in the XHYPERS model are treated fully kinetically with the PIC method. As in the standard (HYPERS) hybrid model, Eq. (4) assumes charge quasineutrality. In XHYPERS, this equation in general can be replaced by a continuity equation for the electron fluid.

The energy outflow from the beam-plasma system is modeled by the collisional term in Eq. (1). It phenomenologically represents the nonlinear conversion of lower-hybrid waves to whistler waves and their radiative convection out of the beam-plasma system, similarly to the previous electrostatic simulations.[11]

In this study, we consider a uniform plasma and neglect the advection term in the electron equation of motion. For simplicity, the electron pressure term is also ignored in this equation since in the

near-Earth region, which is of immediate interest to the SMART experiment, the phase speed of the waves of interest is much larger than the electron thermal speed. This allows us to use the cold plasma limit.

Overall, Eqs. (1)–(4) form a self-consistent hybrid model for describing an electromagnetic quasineutral background plasma response to an ion beam. Since the electrons are modeled as a fluid, the mesh cell size in our simulation is not limited by the Debye length or electron cyclotron scales as in full PIC simulations. We integrate over electron plasma scales using an efficient implicit procedure,[20] which allows us to avoid the time step limitations associated with these fast scales. As a result, our computational model allows much longer simulations of the beam-plasma system compared to equivalent full PIC simulations without sacrificing relevant physics.

B. Multiscale computation

The HYPERS code differs from standard PIC codes by enabling time adaptivity of simulation variables (particles and mesh-discretized fields). This property is achieved by applying a novel approach to time integration, EMAPS (Event-driven Multi-Agent Planning System), formerly referred to as DES (Discrete-Event Simulation).[15] In general, EMAPS greatly facilitates simulations of global multiscale systems by enabling explicit integration of particle trajectories and discrete fields on their own, self-adaptive timescales, which are computed "on the fly" during a simulation as a function of the underlying local physics and mesh properties.

In XHYPERS, the set of Eqs. (1)–(4) is solved implicitly with respect to the fast electron plasma scales [i.e., with respect to $\mathbf{V}_e$ and $\mathbf{E}$ in Eqs. (1) and (2)] and explicitly with respect to the magnetic field, $\mathbf{B}$ in Eq. (3). These equations are currently solved together with a common predefined time step of order a fraction of the CFL (Courant–Friedrichs–Lewy) value for light waves. Particle trajectories, on the other hand, are computed asynchronously, similarly to the HYPERS model. This prevents a small number of faster particles (accelerated by turbulence) from slowing down the overall simulation speed.

C. Simulation setup

The simulations described in this paper have been conducted in a periodic rectangular domain, $64 \times 16 \times 16\, d_e^3$ covered with a uniform Cartesian mesh of $200 \times 50 \times 50$ cells, where $d_e = c/\omega_{pe}$ is the electron inertial length and ω_{pe} is the electron plasma frequency. The external magnetic field is directed along the x-axis. The size of the computational domain is chosen to be large enough to preclude wave mode aliasing, which is manifested in an asymmetric beam relaxation in velocity space for smaller domains.

Singly charged background plasma and beam ion particles were initialized uniformly distributed over the simulation domain, with the beam to background ion density, $n_b/n_i = 0.25$ and 100 particles per cell for each ion species. The electron plasma to cyclotron frequency ratio, $\omega_{pe}/\omega_{ce} = \sqrt{3}$ was chosen to be the same as in the previous full PIC simulations.[12] The background ions were initialized with zero velocities. The beam ions were created with $V_x = 0$ and a ring velocity distribution in the $V_y - V_z$ space, centered around a beam speed, $V_b \simeq 0.004c$, with a Maxwellian thermal spread, $\delta V_b \simeq 0.02\, V_b$.

The characteristic linear growth rate of lower hybrid oscillations is given by an expression derived for a cold ion beam as a function of the background plasma and beam ion masses:[7]

$$\gamma_L \simeq 0.3\omega_{LH}\left(\frac{n_b}{n_e}\frac{M_i}{M_b}\right)^{2/5} \simeq 0.1\omega_{pe}\sqrt{\frac{m_e}{M_b}}\left(\frac{M_i}{M_b}\right)^{2/5}. \tag{5}$$

In this study, we use this growth rate as a characteristic value with respect to which we scale the effective electron damping, ν_e, in our simulations.

III. RESULTS

Using the parameters discussed in Sec. II, we have conducted four runs labeled with Latin numerals, from I though IV. In these runs, we varied the background plasma ion mass, M_i, the beam ion mass, M_b, and the effective electron damping, ν_e, as shown in Table I. This table also summarizes linear growth rates given by Eq. (5) and energy deposition amounts for each run: the ratio of the total energy lost by the beam by the end of the simulation period, $|\Delta W_b|$ to the initial beam energy, W_{b0}; and the ratio of the effective electron dissipated energy, ΔW_e to the total beam energy loss, $|\Delta W_b|$.

The beam ions lose only a fraction of their initial energy to the waves because of their concomitant turbulent heating. The net beam energy loss, $|\Delta W_b|$ is partitioned between the waves, electrons, and background plasma ions. We are interested in determining the fraction of beam energy, ΔW_e deposited into plasma turbulence that escapes the beam-plasma interaction region through the effective electron damping. For simplicity, we assume $\Delta W_e = |\Delta W_b| - \Delta W_i$, where ΔW_i is the energy absorbed by the background ions.

Figures 1 and 2 present time histories of ΔW_b and ΔW_i normalized to the initial beam energy, W_{b0} in the four simulations. Runs I-III use the heaviest background ions, $M_i/m_e = 1836$. In runs I–II, the beam is composed of ions with $M_b/M_i = 4$, while in Run III the beam ions are twice as heavy, $M_b/M_i = 8$.

We note a significant difference in the plasma dynamics in run I and run II (Fig. 1) due to significantly different effective electron damping rates in these (otherwise similar) simulations. A larger effective damping rate in run I results in a smaller relative amount of energy being absorbed by the background ions compared to the electron dissipated energy (see Table I) which mimics in our model the

TABLE I. Summary of parameters and results for five simulation runs: M_i/m_e is the background ion to electron mass ratio; M_b/M_i is the beam to background ion mass ratio; t_{sim} is the total simulation time; ν_e is the effective electron damping rate; γ_L is the linear instability growth rate; ΔW_b is the ion beam energy loss; ΔW_e is the effective electron dissipated energy; W_{b0} is the initial beam energy; ω_{pi}, ω_{pe} are the background ion and electron plasma frequencies, respectively.

Run	I	II	III	IV
M_i/m_e	1836	1836	1836	1024
M_b/M_i	4	4	8	4
$t_{sim}\omega_{pi} \times 10^3$	5.6	5.6	8.6	8.6
$\nu_e/\omega_{pe} \times 10^3$	0.5	0.1	0.5	0.5
$\gamma_L/\omega_{pe} \times 10^3$	1.3	1.3	1.0	1.8
$\lvert\Delta W_b\rvert/W_{b0}(\%)$	8.5	5.0	4.5	8.5
$\Delta W_e/\lvert\Delta W_b\rvert(\%)$	41	28	53	64

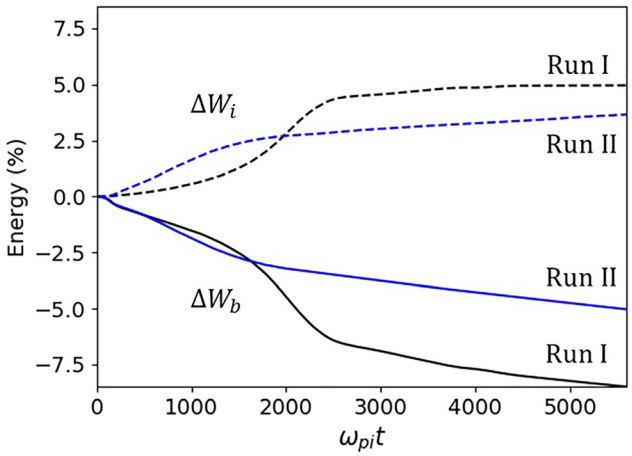

FIG. 1. Time histories of energies absorbed by the background ions, ΔW_i (dashed lines) and lost by the beam ions, ΔW_b (solid lines), as percentage of the initial beam energy, W_{b0} in run I (black color) and run II (blue color).

energy losses due to outgoing whistler waves generated through nonlinear induced electron scattering.[3,8]

Notably, in run I we also observe nonlinear saturation of the background plasma heating rate at $\omega_{pi}t \geq 3000$. At the same time, the beam continues losing energy, which is mostly absorbed by the electrons (see Fig. 1). This scenario creates conditions favorable for efficient energy transfer from the beam to the plasma electrons and waves, when a significant fraction of beam energy is channeled away from both the background plasma and the beam ions.

Further, large plasma ion heating occurs in simulations because all the beam ions deposit their energy simultaneously at the initial moment.[21] This leads to the initially large lower-hybrid wave amplitudes and strong diffusion or even perhaps some nonlinear heating of ions. In the SMART experiment, neutral beam ionization will be gradual. As a result, the beam energy will be released slowly over the long ionization time, which is much larger than the characteristic lower-hybrid wave growth/decay times. Also, as the ionization front moves at speeds of order 10 km/s, new waves will be born in pristine plasma so that the instability threshold conditions will be relatively unaffected by ion heating due to old ions. These processes are not currently simulated in our model and therefore ion heating rates observed in our simulations should be considered as conservative estimates.

The significant reduction of beam relaxation rate in run I is demonstrated in Fig. 3, which illustrates the temporal evolution of the beam ion velocity distribution. Clearly, the relaxation of the beam distribution in velocity space proceeds significantly slower in the second part of the simulation ($\omega_{pi}t \geq 3000$) compared to the earlier stages of the instability.

In contrast, in run II the background ions continue absorbing a considerable portion of beam energy with time, albeit at a rate slower than the overall beam energy extraction rate. No background ion energy saturation is observed during the same period of simulation time as in run I. Therefore, by comparing the results from run I and run II, we conclude that the effective damping γ_e, which describes energy outflow from the beam-plasma system in our model, plays a crucial role in transferring energy from the beam to plasma turbulence.

Overall, the results from run I and run II simulations demonstrate the importance of including the background ion kinetics when studying evolution of the ion ring-plasma system. Since these effects affect the threshold condition for wave generation and compete with the excitation of lower hybrid oscillations by the beam ions, they should be considered together with the nonlinear mechanisms.[3,8] This result is further corroborated by Fig. 2, which shows results from run III ($M_i/m_e = 1836$, $M_b/M_i = 8$) and Run IV ($M_i/m_e = 1024$, $M_b/M_i = 4$).

In simulation III, where the ratio of $M_b/M_i = 8$ is chosen to be close to the realistic ratio of the barium to oxygen ion mass, $M_{Ba}/M_0 \simeq 8.6$, the electrons absorb relatively more energy than in Run I, where the beam ions are lighter. Although in this case the beam energy extraction rate is lower, the background ion heating rate practically zeroes out at $\omega_{pi}t \geq 4000$, while the beam continues to deposit energy into the plasma almost at a constant rate.

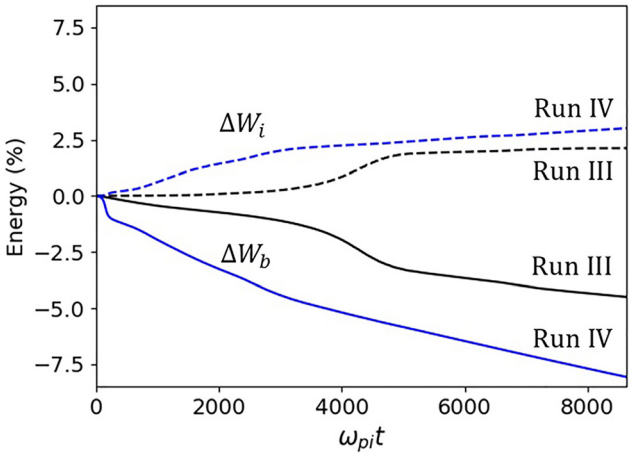

FIG. 2. Time histories of energies absorbed by the background ions, ΔW_i (dashed lines) and lost by the beam ions, ΔW_b (solid lines), as percentage of the initial beam energy, W_{b0} in run III (black color) and run IV (blue color).

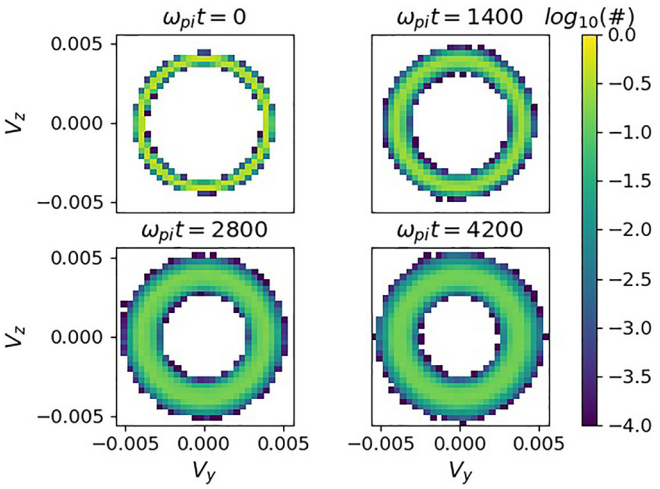

FIG. 3. Time evolution of the beam velocity distribution function in run I.

Figure 2 demonstrates energy time histories for run IV, where the beam and plasma ion masses ($M_i/m_e = 1024$, $M_b/M_i = 4$) were chosen to be identical to those in full PIC simulations[12,13] which were a factor of 10 shorter compared to our simulations.

We observe that at $\omega_{pi}t \simeq 1000$, which corresponds to the end of the full PIC simulation,[13] the beam ions lose in our simulations approximately 2% of its initial energy compared 4% observed in the full PIC simulation. However, taking into account the differences between the hybrid and full PIC models, as well as somewhat different initial beam parameters (e.g., the denser and faster beam in the full PIC case), these numbers can be considered to be sufficiently close.

Both the hybrid (longer) and full PIC (shorter) simulations demonstrate continuous energy extraction from the ion beam with time. We also observe that the relative energy absorption by the plasma electrons in run IV (Table I) is only slightly higher than in the more realistic run III. In addition, as in run II, the background ions in run IV continue to be heated at a finite rate by the end of the simulation.

Finally, Fig. 4 illustrates the differences in lower hybrid wave turbulence in run I and run II, manifested in the form of background plasma density striations of different amplitudes. These striations are much better developed in Run I where the effective electron damping rate is greater. This difference can be explained by recalling that the effective damping in our model represents energy outflow from the beam due to a mechanism missing from our hybrid model, i.e., the conversion of the electrostatic lower hybrid oscillations to the electromagnetic whistler waves, which propagate out of the beam-plasma interaction region.[5,8] In our simulations, this damping mechanism competes with the beam-plasma instability. As a result, the beam ions in Run I diffuse in velocity space (Fig. 3) slower than in Run II (not shown here). Effectively, this makes the instability in Run I proceed unhindered for a longer time compared to Run II, which ultimately results in transferring more energy from the beam to plasma turbulence (Fig. 1).

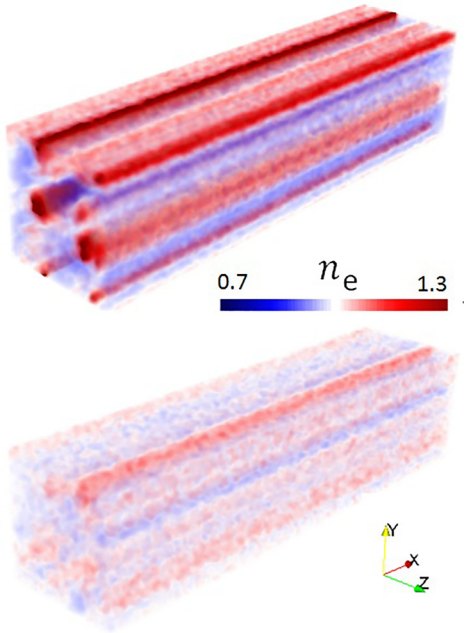

FIG. 4. Plasma electron density normalized to the initial electron density in run I (top) and run II (bottom) at $\omega_{pi}t = 2800$.

IV. SUMMARY

The upcoming *in situ* SMART experiment[5,6] is designed to study the evolution of lower hybrid turbulence excited by a heavy barium ion in unbounded space plasma by space charge detonation. The consequences of this experiment cannot be accurately reproduced in laboratory or simulations. In particular, this experiment will focus on studying the interchangeability between electrostatic and electromagnetic waves and their nonlocal consequences in the near-Earth space environment. It must be emphasized that while the previously used 2D electrostatic PIC model[6] is appropriate for assessing the instability onset and the consequent loss of beam energy in the initial phase, it is not appropriate for the subsequent dynamics that in reality includes conversion of electrostatic lower hybrid waves into electromagnetic whistlers/magnetosonic waves, and their propagation out of the source region, which are critical components of the SMART experiment. In this paper, we have described a numerical investigation of the energy deposition by an ion ring velocity beam in a magnetized plasma at later times. The goal of this study is to estimate the fractions of beam energy deposited into different physical channels, namely into the background plasma electrons and ions.

We advance the previous 2D electrostatic hybrid simulations[11,21] by using a novel electromagnetic model in three dimensions, which is important for modeling long ion ring evolution. Compared to the previous 3D full PIC simulations,[12,13] we have increased the simulation duration to a more realistic interval relevant to the experiment. We could perform simulations with longer durations because our electromagnetic hybrid model employs a reduced (fluid) description for the plasma electrons. We also use heavier plasma and ring ion masses which make our simulations more realistic for the interpretation and analysis of the experimental results.

Compared to full PIC simulations, the hybrid model used in this study lacks the nonlinear mechanisms necessary for transferring the beam extracted energy from originally short wavelength electrostatic to finally long wavelength electromagnetic modes[3,8] which radiate out of the beam-plasma interaction volume. To compensate for this missing physics, we employ a phenomenological electron damping (collisional term) and investigate how it affects the redistribution of plasma-absorbed energy between the background plasma electrons and ions.

The collisional term is a parameterization of a zeroth order effect, which is an additional channel for energy loss by induced scattering. This loss of energy is likely to play a critical role in the evolution of the lower hybrid turbulence but has generally been overlooked in previous simulations. The exact spectral structure may introduce higher order corrections, which are not the immediate focus in this study since such differences may not be measurable in the SMART experiment. Such refinements will be addressed in the future.

It should also be noted that in addition to induced scattering, there exists another nonlinear mechanism for wave energy saturation via modulation instability. The timescale of induced scattering and modulation instability are comparable.[8] However, in the SMART experiment a broadband wave spectrum will be generated. For waves in an incoherent broadband spectrum, it is difficult to maintain the

phase coherence necessary for the nonlinear Schrödinger equation solution to compete with induced scattering. Moreover, induced electron scattering can remove the waves from the density cavity that traps the lower hybrid waves and thereby impede in the formation of coherent structures. This may explain the lack of evidence of plasma heating in the ionosphere[22,23] by the theoretically predicted collapse of lower hybrid solitons.[24]

In our simulations, we have demonstrated the critical dependence of the rate of ion beam energy deposition into lower-hybrid plasma turbulence on the effective electron damping rate, which mimics the effect of induced scattering interactions of plasma electrons with wave turbulence. We have shown that for the realistic beam to background ion mass ratio and a sufficiently large damping rate the energy absorbed by the ions saturates, while the beam continues to deposit a significant fraction of its initial energy into the electrons. In addition, this dissipative channel, which simulates the effect of electromagnetic waves in an unbounded plasma, slows down ion ring relaxation in velocity space. This makes more energy available to the background plasma and electromagnetic waves, rather to the beam ions.

The 3D simulations presented in this paper require significantly less computational resources and run an order of magnitude longer in physical time than equivalent full PIC simulations. This makes the hybrid model a valuable tool for investigating the ion ring beam-plasma instability over long periods of time, which is a useful surrogate for estimating the efficiency of beam energy transfer to the waves. Compared to the previous 2D electrostatic model,[11] the 3D extended hybrid model (XHYPERS) introduced here supports large-amplitude whistlers. Therefore, it can also be applied, for instance, to simulate interactions of energetic electrons (modeled as minority kinetic species) with oblique whistlers.[25]

ACKNOWLEDGMENTS

This work was supported by DARPA. C.C. and G.G. were partially supported by the NRL Base Program. The simulations have been performed on the Pleiades supercomputer at NASA's Ames Research Center. The authors express their gratitude to Li-Jen Chen (NASA GSFC) for extending her group's computational time support to benefit this project.

DATA AVAILABILITY

The data that support the findings of this study are available from the corresponding author upon reasonable request.

REFERENCES

[1] R. L. Stenzel and W. Gekelman, "Electrostatic waves near the lower hybrid frequency," Phys. Rev. A **11**, 2057 (1975).
[2] G. Ganguli, L. Rudakov, M. Mithaiwala, and K. Papadopoulos, "Generation and evolution of intense ion cyclotron turbulence by artificial plasma cloud in the magnetosphere," J. Geophys. Res. **112**, A06231, https://doi.org/10.1029/2006JA012162 (2007).
[3] M. Mithaiwala, L. Rudakov, G. Ganguli, and C. Crabtree, "Weak turbulence theory of the nonlinear evolution of the ion ring distribution," Phys. Plasmas **18**, 055710 (2011).
[4] E. M. Tejero, C. Crabtree, D. D. Blackwell, W. E. Amatucci, G. Ganguli, and L. Rudakov, "Model for nonlinear evolution of localized ion ring beam in magnetoplasma," Sci. Rep. **5**, 17852 (2016).
[5] G. Ganguli, L. Rudakov, W. Scales, J. Wang, M. Mithaiwala, J. Huba, C. Siefring, W. Amatucci, and C. D. Lewis, "Understanding and harnessing the dual electrostatic/electromagnetic character of plasma turbulence in the near-earth space environment," J. Geophys. Res. **124**, 10365–10375, https://doi.org/10.1029/2019JA027372 (2019).
[6] A. Fletcher, C. Crabtree, J. Huba, G. Ganguli, and C. Siefring, "Early time evolution of turbulence in the space environment by neutral beam injection," J. Geophys. Res.: Space Phys. **125**, e2019JA027587, https://doi.org/10.1029/2019JA027587 (2020).
[7] M. Mithaiwala, L. Rudakov, and G. Ganguli, "Stability of an ion-ring distribution in a multi-ion component plasma," Phys. Plasmas **17**, 042113 (2010).
[8] G. Ganguli, L. Rudakov, W. Scales, J. Wang, and M. Mitthaiwala, "Three dimensional character of whistler turbulence," Phys. Plasmas **17**, 052310 (2010).
[9] Y. A. Omelchenko, R. Z. Sagdeev, V. D. Shapiro, and V. I. Shevchenko, "Numerical simulation of quasilinear relaxation of a ring ion beam and of production of superthermal electrons," Sov. J. Plasma Phys. **15**, 427–431 (1989).
[10] E. M. Tejero, C. Crabtree, D. D. Blackwell, W. E. Amatucci, M. Mithaiwala, G. Ganguli, and L. Rudakov, "Laboratory studies of nonlinear whistler wave processes in the Van Allen radiation belts," Phys. Plasmas **22**, 091503 (2015).
[11] W. A. Scales, G. Ganguli, L. Rudakov, and M. Mithaiwala, "Model for nonlinear evolution of localized ion ring beam in magnetoplasma," Phys. Plasmas **19**, 062902 (2012).
[12] D. Winske and W. Daughton, "Generation of lower hybrid and whistler waves by an ion velocity ring distribution," Phys. Plasmas **19**, 072109 (2012).
[13] D. Winske and W. Daughton, "Influence of plasma beta on the generation of lower hybrid and whistler waves by an ion velocity ring distribution," Phys. Plasmas **22**, 022102 (2015).
[14] L. Rudakov, C. Crabtree, M. Mithaiwala, and G. Ganguli, "Analysis of Winske-Daughton 3D electromagnetic particle simulation of ion ring generated lower hybrid turbulence," e-prints arXiv:1211.6392 (2012).
[15] Y. A. Omelchenko and H. Karimabadi, "HYPERS: A unidimensional asynchronous framework for multiscale hybrid simulations," J. Comput. Phys. **231**, 1766–1780 (2012).
[16] Y. A. Omelchenko and H. Karimabadi, "Parallel asynchronous hybrid simulations of strongly inhomogeneous plasmas," in Simulation Winter Conference (WSC) (2014), pp. 3435–3446.
[17] M. Kuznetsova, M. Hesse, and D. Winske, "Kinetic quasi-viscous and bulk flow inertia effects in collisionless magnetotail reconnection," J. Geophys. Res. **103**, 199–213, https://doi.org/10.1029/97JA02699 (1998).
[18] T. Amano, K. Higashimori, and K. Shirakawa, "A robust method for handling low density regions in hybrid simulations for collisionless plasmas," J. Comput. Phys. **275**, 197–212 (2014).
[19] M. Lampe, G. Joyce, W. Manheimer, A. Streltsov, and G. Ganguli, "Quasineutral particle simulation technique for whistlers," J. Comput. Phys. **214**, 284–298 (2006).
[20] C. E. Seyler and M. R. Martin, "Relaxation model for extended magnetohydrodynamics: Comparison to magnetohydrodynamics for dense Z-pinches," Phys. Plasmas **18**, 012703 (2011).
[21] G. Ganguli, C. Crabtree, M. Mithaiwala, L. Rudakov, and W. Scales, "Evolution of lower hybrid turbulence in the ionosphere," Phys. Plasmas **22**, 112904 (2015).
[22] K. Lynch, R. Arnoldy, P. Kintner, and J. Bonnell, "The AMICIST auroral sounding rocket: A comparison of transverse ion acceleration mechanisms," Geophys. Res. Lett. **23**, 3293–3296, https://doi.org/10.1029/96GL02688 (1996).
[23] P. Schuck, G. Ganguli, and P. Kintner, "The role of lower-hybrid-wave collapse in the auroral ionosphere," Phys. Rev. Lett. **89**, 065002 (2002).
[24] V. Shapiro, V. Shevchenko, A. Sharma, K. Papadopoulos, R. Sagdeev, and V. Lebedev, "Lower hybrid turbulence at cometary bow wave and acceleration of cometary protons," J. Geophys. Res. **98**, 1325–1331, https://doi.org/10.1029/92JA01729 (1993).
[25] V. Sotnikov, T. Kim, J. Caplinger, D. Main, E. Mishin, N. Gershenzon, T. Genoni, I. Paraschiv, and D. Rose, "Parametric excitation of very low frequency (VLF) electromagnetic whistler waves and interaction with energetic electrons in radiation belt," Plasma Phys. Controlled Fusion **60**, 044014 (2018).